PERIOD-DEPENDENT DURATION FOR THE WESTERN UNITED STATES

Chih-Hsuan Sung and Norman Abrahamson

Department of Civil & Environmental Engineering
University of California, Berkeley

Abstract

Most duration metrics used to characterize design ground motions are based on the acceleration tie series which reflects the duration of the short-period ground motion but may not reflect the duration of the long-period ground motion. A new period-dependent duration based on the cumulative-squared response of a 50%-damped single-degree-of-freedom oscillator is presented. The period-dependent duration metric shows that for T>1 sec, the duration is systematically larger than the traditional accelerogram-based duration. There is also a large variability of the ratio of the long-period duration to the acceleration-based duration. To develop design time histories for structure sensitive to the long-period ground motion, the long-period duration of the time histories should be considered in the selection process.

Introduction

The damage potential of strong ground motion is mainly characterized by the amplitude of shaking, but the duration of the shaking can also affect the damage potential of the ground motion for some structures. The importance of duration on structural performance depends on the type of structure and the damage measure used, leading to varying conclusions about the significance of duration on the damage to structures (Hancock and Boomer, 2006; Bommer et al., 2009). In addition to the dependence on the type of structure and damage measure, the varying conclusions about the importance of duration on structural response may also be related to the duration metric used. Bommer and Martínez-Pereira (1999) noted that over 30 different definitions duration that had been proposed in the literature.

Duration has two main uses in seismic hazard and ground motion studies. In seismic hazard studies, the main use of duration models is to set the expected duration for the design ground motions which is then used to guide the selection of ground-motion time series for later use in the dynamic analyses of the structure. In ground-motion studies, the duration models are used in the application of random vibration theory (RVT) to convert Fourier Amplitude Spectra (FAS) to response spectral values (Boore and Thompson, 2014).

Currently, the most widely used duration metric is based on the normalized Arias intensity, AI_N, (Arias, 1970):

$$\mathrm{AI}_N(\mathrm{t}) = \frac{\int_0^t a^2(\tau)d\tau}{\int_0^{tmax} a^2(\tau)d\tau} \quad (1)$$

in which AI_N is the normalized Arias Intensity, and $a(\tau)$ is the acceleration time series. Equation (1) can be inverted to give the time as a function of the AI_N. The significant duration is defined as the time between the AI_N reaches two selected percentages, X and Y:

$$D_{X-Y} = t(AI_N - Y) - t(AI_N - X) \quad (2)$$

The $t(AI_N - X)$ is the time at which the normalized Arias intensity is equal to X. For example, the time between the AI reaching 5% of the total and 75% of the total is called the $D_{5\text{-}75}$ duration.

Multiple empirical models for the $D_{5\text{-}75}$ and $D_{5\text{-}95}$ duration based on the normalized AI have been developed over the years. Recent duration models, such as Afshari and Stewart (2016), Du and Wang (2017)} which are based on the NGA-W2 data set (Ancheta et al, 2014), are commonly used in California seismic hazard studies. These models give the duration for the $D_{5\text{-}75}$ and $D_{5\text{-}95}$. By using the acceleration time series to define duration for the design ground motion, there is an implicit assumption that acceleration duration represents the duration of the ground motion for the period of interest for the structure. That is, the assumption is that the ground-motion duration is the same for all periods. As shown below, this assumption does not hold for long-period ground motion (T>1 sec). In this paper, we propose a period-dependent duration metric that can be used to develop a duration spectrum to complement the response spectrum.

Period-Dependent Duration

One approach to the period dependence of duration is to develop duration models for velocity and displacement time series, analogous to the current approach used for acceleration by simply substituting the velocity or displacement time series for the acceleration time series in equation (2). As an example, the acceleration, velocity, and displacement time series for the Sunland - Mt Gleason Ave recording of the 1994 Northridge earthquake (M=6.7, R_{RUP}=13 km, V_{S30}=446 m/s) is shown in Figure 1. For this recording, the $D_{5\text{-}75}$ duration values for the velocity and displacement time series are longer than for the acceleration time series. The drawback of this approach is the predominate period for velocity depends on magnitude: the predominate periods of velocity and displacement are longer for larger magnitude earthquakes. As a result, the duration for velocity for moderate-magnitude earthquakes will sample a different period range than for large-magnitude earthquakes, making it more difficult to develop a simple empirical model that captures the period dependence of the duration using velocity time series.

To directly address the period dependence of duration, we use the cumulative-squared acceleration of the response of a high-damped (50% damping) single-degree of freedom (SDOF) oscillator. That is, we replace the acceleration time series with the time series of the 50%-damped SDOF response. A large damping value is used so that the duration of the response of the SDOF represents the duration of the input ground motion and is less affected by the elongated duration due to the oscillator response. For a spectral period of T=0 sec, the SDOF response is equal to the acceleration time series, so the duration for T=0 will be the same as the current duration metric based on the AI_N. A related period-dependent intensity measure was proposed by Travasarou (2003) in which the period-dependent Arias intensity was computed

from the SDOF response at 5% damping. The main difference between these two metrics is that we use a much larger damping, and we use the normalized Arias intensity.

Using the same Sunland recording from the Northridge earthquake, the time series of the response of a 50%-damped SDOF oscillator is shown in Figure 2 for five spectral periods. Similar to the increase in duration for the velocity and displacement time series shown in Figure 1, there is an increase in the duration for the two longer periods for this recording. Computing the duration of the high-damped oscillator for a range of spectral periods, we develop the period dependence of the $D_{5\text{-}75}$ shown in Figure 3. This represents a duration spectrum.

For this recording, the $D_{5\text{-}75}$ duration is nearly constant for periods up to 1 sec and then increases rapidly: the $D_{5\text{-}75}$ duration increases from about 5 sec at short periods to 16-18 sec at long periods (T=2 to T=7 sec), likely due to trapped basin waves in the San Fernando basin. This increase in the duration at long periods is not seen for all recordings. For example, the duration spectra for two recordings from the Northridge earthquake with similar rupture distances of about 15 km are shown in Figure 4. These two recordings have similar $D_{5\text{-}75}$ duration values for the traditional acceleration-based duration (i.e., the period-dependent duration for T=0 sec), but they have very different $D_{5\text{-}75}$ duration values for long periods. This highlights a key limitation of using only the duration based on the Arias Intensity for selecting time histories for dynamic analyses of structures: if the target $D_{5\text{-}75}$ duration was 5-6 sec, both of these recordings would satisfy the Arias Intensity-based duration, but they may lead to very different responses for geotechnical system with a natural period of 2 sec or more, such as large tailings dams, or for building response if the building has a long natural period and the structural response measure is duration sensitive.

The differences in the period-dependent durations and the acceleration duration for a larger set of recordings from the 1994 Northridge earthquake are shown in Figure 5. The durations at long periods tend to be larger than the acceleration durations, but there is large variability in the differences. In some cases, the long-period duration is shorter than the acceleration duration, indicating the long-period ground motion is dominated by a pulse motion. The large variability again highlights the need to consider the long-period duration of candidate ground motions when selecting time series for use in dynamic analyses of structures.

An alternative approach to using the response of a high-damped SDOF would be to bandpass filter the accelerograms and compute the duration of the AI_N for the filtered accelerogram. A disadvantage of this approach is that for frequency bands with low amplitude, the filtered ground motion will tend to look like noise with durations that depend on the length of the recording. Using the response of the SDOF provides provides the effect of bandpass filtering but also reflects the amplitudes. Another advantage is that at very short periods (T=0), the duration of the SDOF becomes equal to the acceleration duration. Using the SDOF response provides duration values at different spectral periods that fits with the spectral periods used for the amplitude of the ground motion based on the response spectrum.

This report provides a summary of the period-dependent duration model for the Western United States. A more detailed description of the development of the model is given in Sung et al. (2025).

Data Set

For the preliminary period-dependent duration model presented at the October 2024 SMIP annual meeting, we used the NGA-W1 data set for which the full set of time series were available to compute the period-dependent duration. For the final model presented in this report, we expanded the data set to include recent recordings from California earthquakes with M>6 in the CSMIP data set and global earthquakes with M>6.5. We also added data from smaller magnitude events in the Western United States available in the NGA-W2 dataset (Ancheta et al., 2014) and NGA-W3 dataset (Buckreis and Stewart, 2025). The magnitude and distance distribution for the data set is shown in Figure 6.

Conditional Model for Period-Dependent Duration

There are two main approaches to developing ground-motion models (GMMs): (1) the traditional approach based on independent parameters such as magnitude, distance, and site condition and (2) the conditional GMM approach that includes a measure of the ground motion as an input parameter (Macedo et al., 2022). We use the conditional model for period-dependent duration for earthquakes in active crustal regions with the traditional $D_{5\text{-}75}$ and $D_{5\text{-}95}$ acceleration duration (i.e., the duration for T=0 sec) used as an input parameter, denoted $D_{5\text{-}75,acc}$ and $D_{5\text{-}95,acc}$, respectively. The general form of the conditional GMM for the median period-dependent duration is given by:

$$D_{5-X}(T) \;=\; f_1(M, R, V_{S30}) \;+\; f_2(D_{5-X,acc}) \tag{3}$$

in which the $D_{5-X,acc}$ is traditional duration of the accelerogram, X is either 75 or 95, and the $f_1(M, R, V_{S30})$ term reflects the differences in the magnitude, distance, and site scaling for the $D_{5-X,acc}$ and the $D_{5-X}(T)$. A preliminary analysis showed that the magnitude dependence of $f_1(M, R, V_{S30})$ was not significant. That is, the magnitude scaling for the period-dependent duration is captured in the magnitude scaling of the $D_{5-X,acc}$ values. Therefore, we only included the distance and V_{S30} dependence in the initial model for f_1.

For duration, the source, path, and site effects are additive, not multiplicative as for response spectral values (Pinilla-Ramos et al., 2024). We used a power-normal transformation for the duration, consistent with the Pinilla-Ramos et al. (2024) duration model for the acceleration duration. The functional for the conditional model is given by:

$$D_{5-X}^{0.3}(T, R_{RUP}, V_{S30}) = [D_{Site}(T, V_{S30}) + c_5 D_{5-X,\mathrm{acc}}(T) + D_{Path}(T, R_{RUP})]^{0.3} + \delta, \tag{4}$$

in which R_{RUP} is the rupture distance in km, V_{S30} is the time-averaged shear-wave velocity over the top 30 m in m/s, and $D_{5-X,ACC}$ is the duration measured from the normalized Arias Intensity (AI_N) in sec. The δ are the residuals in units of $sec^{0.3}$ and are assumed to be normally distributed with mean 0 and standard deviation $\sigma_{D(T)}$. The site and path terms are given by:

$$D_{Site}(T, V_{S30}) = c_4(T) ln\left(\frac{Min(V_{S30}, 1000)}{2000}\right) \tag{5}$$

and

$$D_{Path}(T, R_{RUP}) = c_7(T, R_{RUP}) R_{RUP} \tag{6}$$

in which

$$c_7(T, R_{RUP}) = \begin{cases} c_{71} & \text{for } R_{RUP} \leq R_2 \\ c_{71}(T) + \frac{c_{72}(T) - c_{71}(T)}{R_4 - R_2}(R_{RUP} - R_2) & \text{for } R_2 < R_{RUP} \leq R_4 \\ c_{72}(T) & \text{for } R_{RUP} > R_4. \end{cases} \tag{7}$$

The residuals from a regression using this initial model showed a systematic negative bias (overprediction) at short distances (R_{RUP} < 10 km). Because the short distance range is an important range for applications of the model, the c_4 and c_7 terms were modified at short distances to reduce the overprediction. The form for the modified c_4 and c_7 terms are shown in Equations (8) and (9).

$$c_{4,mod}(T, R_{RUP}) = \begin{cases} 0 & \text{for } R_{RUP} \leq R_1 \\ \frac{c_4(T)}{R_2 - R_1}(R_{RUP} - 3) & \text{for } R_1 < R_{RUP} \leq R_2 \\ c_4(T) & \text{for } R_{RUP} > R_2, \end{cases} \tag{8}$$

$$c_{7,mod}(T, R_{RUP}) = \begin{cases} 0 & \text{for } R_{RUP} \leq R_1 \\ \frac{c_{71}(T,M)}{R_2 - R_1}(R_{RUP} - R_1) & \text{for } R_1 < R_{RUP} \leq R_2 \\ c_{71}(T, M) + \frac{c_{72}(T) - c_{71}(T,M)}{R_4 - R_2}(R_{RUP} - R_2) & \text{for } R_2 < R_{RUP} \leq R_4 \\ c_{72}(T) & \text{for } R_{RUP} > R_4. \end{cases} \tag{9}$$

We set both $c_{4,mod}$ and $c_{7,mod}$ to 0 for distances less than R_1 (3 km), which is consistent with our finding that $D_{5\text{-}X,acc}$ accounts for both the short-period and long-period duration for short distances.

In addition, the residuals showed a negative bias for small magnitudes (M<5.5) at intermediate distances (10-50 km). An additional path term, $c_{73} R_{RUP}$, was added to account for the smaller duration at long periods for small magnitude earthquakes at intermediate distances:

$$c_{73}(T, M, R_{RUP}) = \begin{cases} 0 & \text{for } R_{RUP} \leq 10km \\ c_{73,adj}(T, M) - \frac{c_{73,adj}(T,M)}{10-R_2}(R_{RUP} - R_2) & \text{for } 10km < R_{RUP} \leq R_2 \\ c_{73,adj}(T, M) - \frac{c_{73,adj}(T,M)}{R_3-R_2}(R_{RUP} - R_2) & \text{for } R_2 < R_{RUP} \leq R_3 \\ 0 & \text{for } R_{RUP} > R_3. \end{cases} \quad (10)$$

in which the $c_{73,adj}$ term applies a magnitude taper to limit the $c_{71,adj}$ term to smaller magnitudes (M<5.5):

$$c_{73,adj}(T, M) = \begin{cases} c_{71,adj} & \text{for } M \leq 4.5 \\ c_{71,adj} - c_{71,adj}(R_{RUP} - 4.5) & \text{for } 4.5 < M \leq 5.5 \\ 0 & \text{for } M > 5.5 \end{cases} \quad (11)$$

The final model is given by:

$$D^{0.3}_{5-X}(T, M, R_{RUP}, V_{S30}) = [c_{4,mod}(T, R_{RUP}) ln\left(\frac{Min(V_{S30}, 1000)}{2000}\right) + c_5 D_{5-X,\text{acc}}(T) + c_{7,mod}(T, R_{RUP}) R_{RUP} + c_{73}(T, M, R_{RUP}) R_{RUP}]^{0.3} + \delta, \quad (12)$$

The period dependence of the smoothed coefficients for $D_{5\text{-}75}$ and $D_{5\text{-}95}$ are shown in Figure 5. For both $D_{5\text{-}75}$ and $D_{5\text{-}95}$, the significant period dependence starts for T>0.5 sec. The c_5 is between 0.9 and 1.0 for T<4 sec indicating that the $D_{5-X}(T)$ has similar scaling with magnitude, distance, and site condition as the traditional $D_{5-X,acc}$ metric. Comparing the coefficients for $D_{5\text{-}75}$ and $D_{5\text{-}95}$, the distance scaling is stronger for the $D_{5\text{-}95}$, whereas the V_{S30} scaling is stronger for the $D_{5\text{-}75}$. indicating that the effects of scattering in the crust along the ray path are more important for the duration from 75% to 95% part of the seismogram than for the 5-75% part. For $D_{5\text{–}75}$(T), the $c_{71,\text{adj}}$ term is negative at longer periods which reduces the distance scaling for small magnitude events. For $D_{5\text{–}95}$(T), the path-duration from the c_7 term captures the distance scaling, so the $c_{71,\text{adj}}$ term is set to zero for all periods.

The total residuals for T=3 sec and T=5 sec for the $D^{0.3}_{5-75}$ and $D^{0.3}_{5-95}$ are shown as a function of distance in Figure 8. The mean residuals for distance bins, shown by the pink points, are centered on zero. The durations from the 2023 Turkey mainshock were not included in the regression and are used as a check of the model. The residuals from the 2023 Turkey mainshock are shown by the red crosses in Figure 8. At short distances (less than 5 km), the residuals at T=3 and T=5 sec for the 2023 Turkey mainshock tend to be negative (the model overpredicts long-period duration). For this event for T=3, the mean residual for the $D^{0.3}_{5-75}$is about -0.5 which corresponds to a reduction of the median duration from about 10.5 sec from the model to 7.3 sec for this event. The smaller duration is related to forward directivity effects that lead to velocity

pulses and shorter durations for the long-period ground motion. For comparison, Pinilla-Ramos et al. (2024) showed that the acceleration durations at short distances for the 2023 Turkey mainshock were not biased low. To keep the duration model simple, we have not incorporated directivity parameters into the current period-dependent duration model, but this may be an area for future improvement.

Scaling of the Period-Dependent Duration

The distance scaling of the $D_{5\text{-}75}(T)$ and $D_{5\text{-}95}(T)$ is shown in Figure 9 for M=7 and V_{S30}=400 m/s. At short distance (1 km), the $D_{5\text{-}X}(T)$ at long periods is smaller than the $D_{5\text{-}X,acc}$ duration, indicating that the long-period energy tends to be packed into a pulse at this very short distance. At moderate and large distances, $D_{5\text{-}X}(T)$ becomes larger than $D_{5\text{-}X,acc}$ for periods greater than 0.5 sec. The distance scaling at long periods is stronger than the distance scaling for the acceleration duration, as shown by the wider range of durations at the long periods than at the short periods.

The V_{S30} scaling of the $D_{5\text{-}75}(T)$ and $D_{5\text{-}95}(T)$ is shown in Figure 10 for M=7 and R_{RUP}=15 km. For the $D_{5\text{-}75}(T)$, the V_{S30} scaling is stronger for long periods than for the acceleration duration, but for the $D_{5\text{-}95}(T)$, the V_{S30} scaling at long period is similar to the V_{S30} scaling for the acceleration duration. This indicates that the contribution from the 75-95% range in the $D_{5\text{-}95}(T)$ is more affected by the scattering along the ray path than by the site effect on the duration.

The magnitude scaling of the $D_{5\text{-}75}(T)$ and $D_{5\text{-}95}(T)$ is shown in Figure 11 for R_{RUP}=15 km and V_{S30}=400 m/s and is shown in Figure 12 for R_{RUP}=15 km and V_{S30}=400 m/s. The magnitude scaling of the duration at long periods is weaker than the magnitude scaling at short periods, indicating that the effects of scattering of long-period waves are dominating the duration over the finite-source duration effects.

Standard Deviation Model

The standard deviation of the conditional duration model is both magnitude and distance dependent and is modeled by the following form:

$$ln(\sigma_{D(T)|D_{acc}})(T) = a_0(T) + a_1(T)(M-6) + b_1(T)(R_{RUP}/100) \quad (13)$$

The model is developed for $ln(\sigma_{D(T)|D_{acc}})$ to restrict the standard deviation to be greater than zero. The coefficients $a_0(T)$, $a_1(T)$ and $b_1(T)$ are listed in Tables 6 and 7 for $D_{5\text{-}75}$ and $D_{5\text{-}95}$, respectively. The period dependence of the coefficients is shown in Figure 13. The magnitude dependence shows greater variability of long-period duration from small-magnitude earthquakes as compared to large-magnitude earthquakes. This reflects the additive form of the duration model (source + path + site) as compared to the multiplicative form (source x path x site) for ground-motion amplitudes. The large magnitude earthquakes have a large source term which tends to reduce the effect of the variability of the path term on the variability of the total duration.

The standard deviation for the duration for a given scenario is computed by considering both the variance of the conditional model and the variance of the acceleration duration given by Pinilla-Ramos et al., (2024).

$$VAR(D^{0.3}_{5-X}(T)) = VAR(D^{0.3}_{5-X}(T)|D^{0.3}_{5-X,acc}) + \left(\frac{\partial D^{0.3}_{5-X}(T)}{\partial D^{0.3}_{5-X,acc}}\right)^2 VAR(D^{0.3}_{5-X,acc}) \quad (14)$$

in which

$$\frac{\partial D^{0.3}_{5-X}(T)}{\partial D^{0.3}_{5-X,acc}} = 0.3[D_{Site}(T, V_{S30}) + c_5 D_{5-X,\mathrm{acc}} + D_{Path}(T, R_{RUP})]^{-0.7}(3.33\, c_5 D^{0.7}_{5-X,acc}) \quad (15)$$

and $D_{5-X,acc}$ is the median acceleration duration given by Pinilla-Ramos et al., (2024).

Example Application

As an example application of the period-dependent duration model, we consider a scenario with M=7, strike-slip, R_{RUP}=15 km, and V_{S30}=270 m/s. The response spectrum is computed for the 84th percentile ground motion (left frame in Figure 15). Given this scenario and response spectrum, the period-dependent duration is computed by first computing the traditional $D_{5\text{-}75\text{-}acc}$ and $D_{5\text{-}95\text{-}acc}$ values using the Pinilla-Ramos et al. (2024) duration model. The Pinilla-Ramos et al. (2024) model includes the negative correlation between the epsilon at the PGA and the duration. This example is for the 84th percentile ground motion, so ε_{PGA}= 1. The median $D_{5\text{-}75\text{-}acc}$ and $D_{5\text{-}95\text{-}acc}$ values are used as inputs to the conditional period-dependent duration models to compute the median and standard deviations for the $D_{5\text{-}75}$(T) and $D_{5\text{-}95}$(T). The resulting 16th, median, and 84th percentile values for the duration spectra for $D_{5\text{-}75}$(T) and $D_{5\text{-}95}$(T) are shown in the center and right frames of Figure 15. These duration spectra can be used to set the target range of the duration for the development of time histories for inputs to the dynamic analyses of the structure. Using this target range for the period-dependent duration will help to avoid selecting time histories with long-period durations that are not centered on the target range.

Implementation Tools

A spreadsheet for implementing the period-dependent duration model is available at github.com/abrahamson/Duration. The spreadsheet uses the Pinilla-Ramos et al. (2024) duration model for the acceleration duration. The inputs to the spreadsheet are the magnitude, rupture distance, V_{S30}, and the ε_{PGA}. The ε_{PGA} is an input for the Pinilla-Ramos et al. (2024) duration model that accounts for the negative correlation between the residuals of the acceleration duration and the residuals of the peak acceleration.

A FORTRAN program for computing the period-dependent duration for a time series is also available github.com/abrahamson/Duration.

Conclusions

The widely used duration based on the normalized Arias Intensity only reflects the duration of the short-period ground motion. The duration for long-period ground motion tends to

be longer than the acceleration-based duration, but there is large variability. For a specific recording, the long-period duration can be smaller than the short-period duration, or it can be much larger than the short-period duration. To develop duration criteria for design ground motions, the period-dependent duration model can be used to develop design spectra for the duration that complement the standard design response spectra design. This will allow selection of ground motions with appropriate durations for dynamic analyses of long-period structures. This may lead to more consistent conclusions about the effect of duration on the structural response

Another use of duration is converting Fourier Amplitude Spectra (FAS) ground-motion models to response spectra models using RVT. In current applications, the amplitude has assumed that ground motion duration is the same for all spectral periods (Kottke et al., 2021; Phung and Abrahamson, 2023). Using a period-dependent duration of the ground motion may improve the accuracy in converting FAS to response spectra.

References

Afshari, K. and J. Stewart (2016). Physically Parameterized Prediction Equations for Significant Duration in Active Crustal Regions, *Earthquake Spectra* Vol 32(4): 2057–2081.

Ancheta, T., R. Darragh, J. Stewart, E. Seyhan, W. Silva, B. Chiou, K. Wooddell, R. Graves, A. Kottke, D. M. Boore, T. Kishida, and J. Donahue (2014). NGA-West2 database, *Earthquake Spectra* Vol 30(3): 989–1005.

Arias, A. (1970). A measure of earthquake intensity, Seismic Design for Nuclear Power Plant - Cambridge, MA: MIT Press, 438–483.

Buckreis, T. and J. Stewart (2025). Data Resources for NGA-West3 Project, Gerrick Institute for Risk Sciences, Report GIRS-2025-07. DOI: 10.34948/N3D30R

Bommer, J. J. and A. Martínez-Pereira (1999). The Effective Duration of Earthquake Strong Motion. *Journal of Earthquake Engineering*, Vol *3*(2): 127–172.

Bommer, J.J., P. J. Stafford, and J.E. Alarcón (2009). Empirical Equations for the Prediction of the Significant, Bracketed, and Uniform Duration of Earthquake Ground Motion, *Bull. Seismol. Soc. Am.,* 2009, Vol 99(6): 3217–3233.

Boore, D. and E. Thompson (2014). Path Durations for Use in the Stochastic-Method Simulation 276 of Ground Motions, *Bull. Seismol. Soc. Am.*, Vol 104(5): 2541–2552.
Du, W. and G. Wang (2017). Prediction equations for ground-motion significant durations using the NGA-West2 Database, *Bull. Seismol. Soc. Am.* Vol 107(1): 319–333.
Du, W. and G. Wang (2017). Prediction equations for ground-motion significant durations using the NGA-West2 Database, Bull. Seismol. Soc. Am. 107(1), 319–333.
Hancock, J. and J. Bommer. (2006). A State-of-Knowledge Review of the Influence of Strong-Motion Duration on Structural Damage. *Earthquake Spectra*. Vol 22(3): 827–845.

Kottke, A., N. Abrahamson, D. Boore, Y. Bozorgnia, C. Goulet, J. Hollenback, T. Kishida, O. Ktenidou, E. Rathje, W. Silva, E. Thompson, and X. Wang, (2021). Selection of random vibration theory procedures for the NGA-East project and ground-motion modeling, *Earthquake Spectra*, July 2021, Vol 37(1_suppl): 1420–1439.

Macedo, J., C. Liu, and N. Abrahamson (2022). On the interpretation of conditional ground-motion models, *Bull. Seismol. Soc. Am.*, Vol: 112(5), pp. 2580-2586.

Phung, V-B. and N. Abrahamson (2023). Conditional Ground-Motion Model Based on RVT Spectral Moments for Converting Fourier Amplitude Spectra to Response Spectra, *Bull Earthquake Eng*, Vol. 21: 5175–5207**.**

Pinilla-Ramos, C., N. Abrahamson, V-B Phung, R. Kayan, and P. Castellanos-Nash (2024). Ground-motion model for significant duration constrained by seismological simulations, *Bull. Seismol. Soc. Am.*, Vol. 114 (2): 1015–1032

Sung, C-H., N. Abrahamson, and G. Lavrentiadis (2025). Period-Dependent Duration for Western North America, *Earthquake Engineering and Structural Dynamics*, In Review

Travasarou, T. (2003). Optimal ground motion intensity measures for probabilistic assessment of seismic slopes displacements, PhD Dissertation, University of California, Berkeley.

Acknowledgements

This study was funded by the SMIP XXXX. The period-dependent durations for the NGA-W2 and NGA-W3 data used in this study were provided by Grigorios Lavrentiadis.

Table 1. CISN Ground-Motion Data with M>=6 and Rupture Distance < 200 km from 2012-2023.

Earthquake Name	Year	Magnitude	Number of Candidate Recordings
Ferndale	2022	6.4	105
Petrolia	2021	6.2	98
Antelope Valley	2021	6.0	367
Ridgecrest	2019	7.1	465
Ridgecrest (foreshock)	2019	6.4	456
South Napa	2014	6.0	109
Ferndale	2014	6.8	30

Table 2. Number of Records and Events in the Dataset (excludes the 2023 Turkey M7.8 main shock)

Region	Magnitude Range	Number of Records	Number of Events
Western US (NGA-W2)	3.0 - 7.4	12,785	375
Western US (NGA-W3)	3.0 - 7.1	38,036	624
Other Regions (NGA-W2)	6.5 - 7.9	454	16
Other Regions (NGA-W3)	6.5 - 7.7	910	19

Table 3. Period-Dependent Coefficients for the Median $D_{5\text{-}75}(T)$ Model.

Period(s)	c_4	c_5	c_{71}	c_{72}	c_{71adj}
0.01	0	1	0	0	0
0.02	0	0.999	0.001	0	-0.001
0.05	0	0.994	0.002	0.001	-0.002
0.075	0	0.992	-0.001	0.001	0.001
0.10	-0.003	0.994	-0.004	0	0.004
0.15	-0.111	0.988	-0.003	-0.002	0.003
0.20	-0.190	0.977	-0.003	-0.003	0.003
0.30	-0.402	0.956	-0.004	-0.006	0.004
0.40	-0.613	0.938	-0.003	-0.006	0.003
0.50	-0.800	0.927	0.004	-0.004	-0.004
0.75	-1.281	0.912	0.018	0.001	-0.018
1.0	-1.589	0.908	0.034	0.007	-0.034
1.5	-1.781	0.906	0.069	0.015	-0.069
2.0	-1.649	0.903	0.100	0.024	-0.100
3.0	-1.645	0.905	0.153	0.049	-0.153
4.0	-1.646	0.900	0.162	0.067	-0.162
5.0	-1.663	0.900	0.154	0.067	-0.154
7.5	-1.689	0.900	0.118	0.038	-0.118
10.0	-1.597	0.900	0.089	0.021	-0.089

Table 4. Period-Dependent Coefficients for the Median $D_{5\text{-}95}(T)$ Model.

Period(s)	c_4	c_5	c_{71}	c_{72}	c_{71adj}
0.01	0	1.000	0	0	0
0.02	0	0.999	-0.0022	-0.0024	0
0.05	0	0.993	-0.0020	-0.0022	0
0.075	0	0.995	-0.0030	-0.0021	0
0.10	0	0.992	-0.0042	-0.0026	0
0.15	-0.001	0.996	-0.0048	-0.0033	0
0.20	-0.115	0.996	-0.0050	-0.0041	0
0.30	-0.247	0.992	-0.0022	-0.0047	0
0.40	-0.416	0.992	0.0024	-0.0041	0
0.50	-0.597	0.985	0.0071	-0.0025	0
0.75	-1.140	0.981	0.0175	0.0026	0
1.0	-1.519	0.965	0.1083	0.0308	0
1.5	-1.782	0.943	0.1717	0.0650	0
2.0	-1.844	0.918	0.2187	0.0959	0
3.0	-1.806	0.900	0.2963	0.1454	0
4.0	-1.881	0.900	0.3088	0.1710	0
5.0	-1.819	0.900	0.3126	0.1729	0
7.5	-1.751	0.900	0.3084	0.1389	0
10.0	-1.789	0.900	0.2812	0.1103	0

Table 5. Period-Independent Coefficients for the $D_{5\text{-}75}(T)$ and $D_{5\text{-}95}(T)$ Median Models

Coefficient	$D_{5\text{-}75}(T)$	$D_{5\text{-}95}(T)$
R_1	3 km	3 km
R_2	20 km	5 km
R_3	50 km	50 km
R_4	150 km	150 km

Table 6. Period-Dependent Coefficients for the Standard Deviation of the $D_{5\text{-}75}(T)$ Model.

Period (sec)	a_0	a_1	b_1
0.01	-9.864	-0.115	-0.546
0.02	-5.075	-0.437	-0.106
0.05	-3.998	-0.303	-0.139
0.075	-3.415	-0.305	-0.327
0.10	-2.911	-0.262	-0.392
0.15	-2.538	-0.306	-0.293
0.20	-2.328	-0.310	-0.225
0.30	-2.003	-0.246	-0.119
0.40	-1.787	-0.195	-0.076
0.50	-1.644	-0.166	-0.057
0.75	-1.459	-0.135	-0.031
1.0	-1.352	-0.115	-0.015
1.5	-1.213	-0.090	-0.007
2.0	-1.130	-0.079	-0.005
3.0	-1.081	-0.070	0.022
4.0	-1.072	-0.065	0.039
5.0	-1.084	-0.046	0.071
7.5	-1.068	-0.007	0.099
10.0	-1.159	0.019	0.178

Table 7. Period-Dependent Coefficients for the Standard Deviation of the $D_{5\text{-}95}(T)$ Model.

Period (sec)	a_0	a_1	b_1
0.01	-11.272	-0.097	0.595
0.02	-5.228	-0.296	0.725
0.05	-4.270	-0.533	0.424
0.075	-3.99	-0.538	0.235
0.10	-3.673	-0.462	0.188
0.15	-3.170	-0.437	0.033
0.20	-2.775	-0.391	-0.056
0.30	-2.247	-0.299	-0.114
0.40	-1.936	-0.235	-0.121
0.50	-1.727	-0.200	-0.125
0.75	-1.445	-0.141	-0.100
1.0	-1.422	-0.115	-0.031
1.5	-1.263	-0.037	-0.026
2.0	-1.187	-0.018	-0.016
3.0	-1.132	0.015	0.010
4.0	-1.087	0.030	0.010
5.0	-1.071	0.042	0.023
7.5	-0.968	0.085	0.023
10.0	-0.958	0.115	0.065

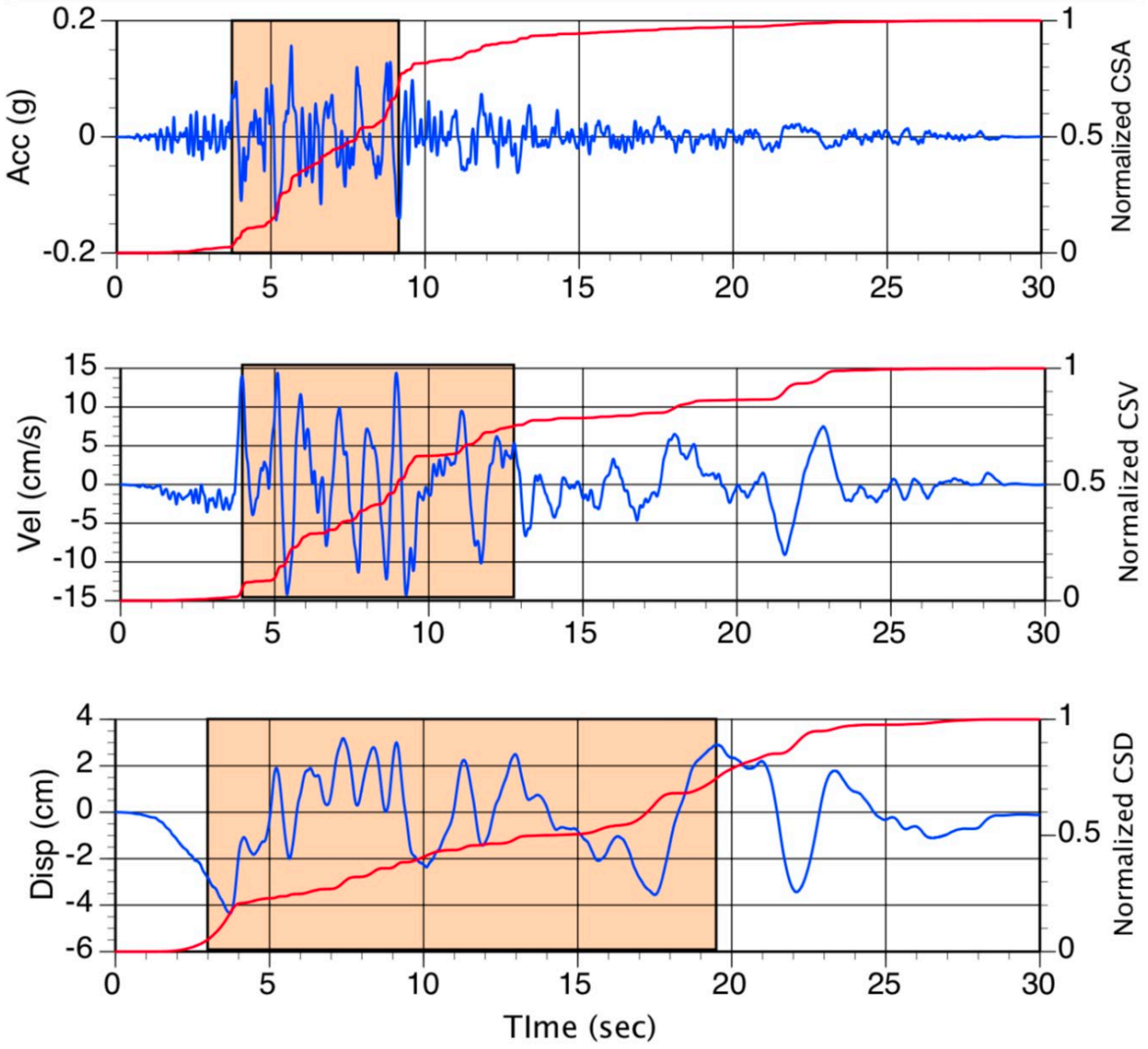

Figure 1. Example of the duration measured from the acceleration, velocity, and displacement time series.

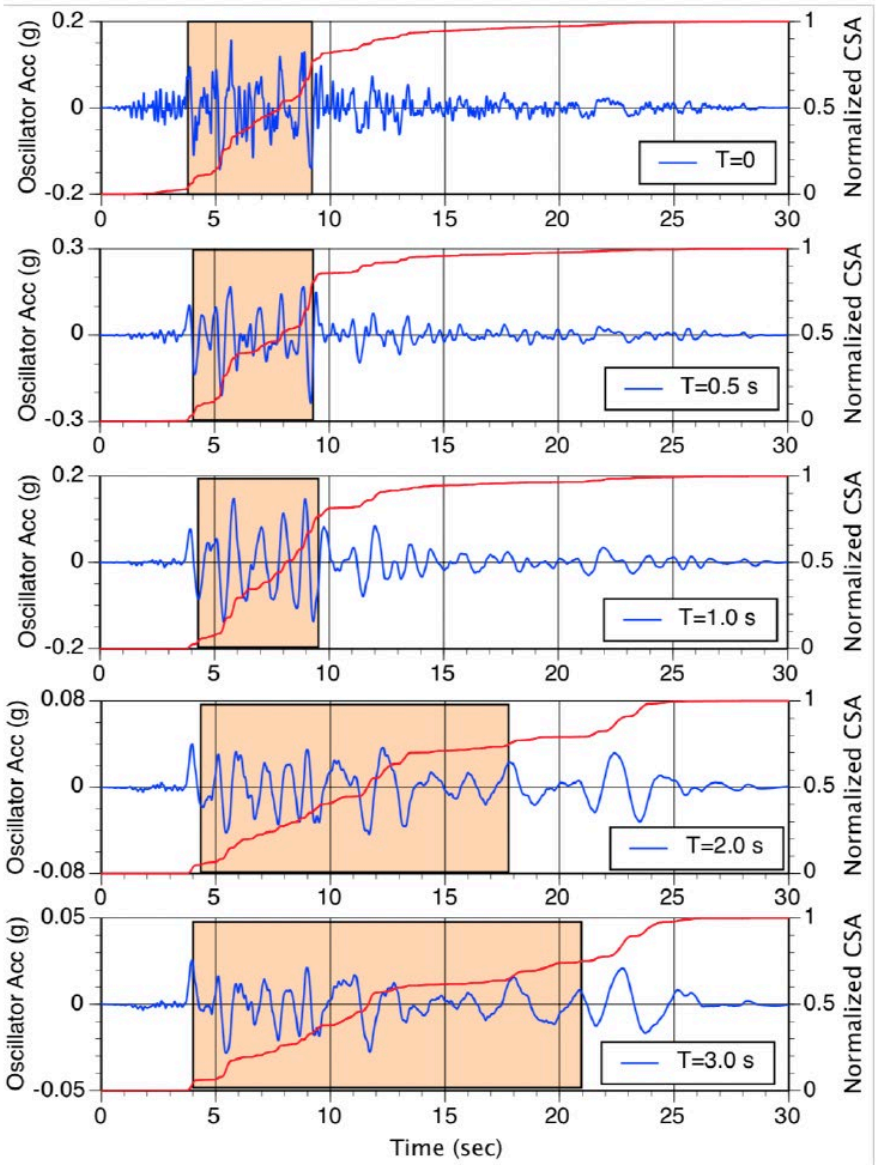

Figure 2. Example of the duration measured from the response of a 50%-damped SDOF for a range of oscillator periods.

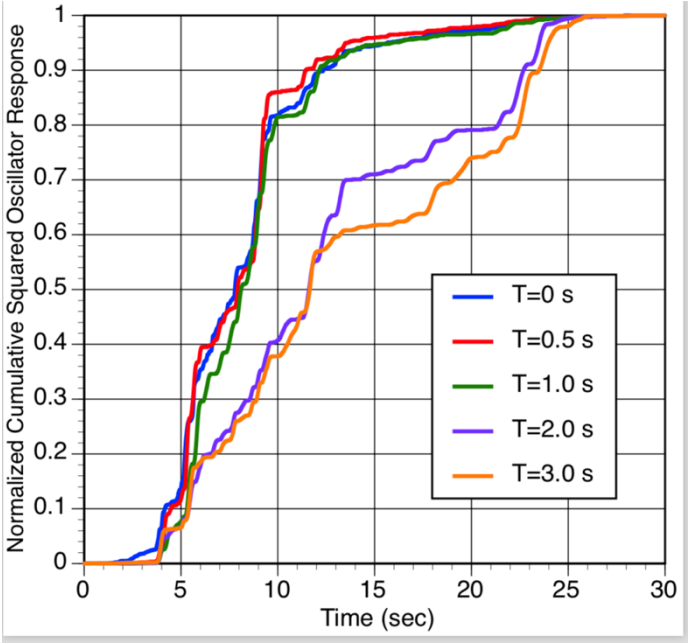

Figure 3. Normalized cumulative-squared response for a 50%-damped SDOF for the Sunland recording from the 1994 Northridge earthquake shown in Figure 2.

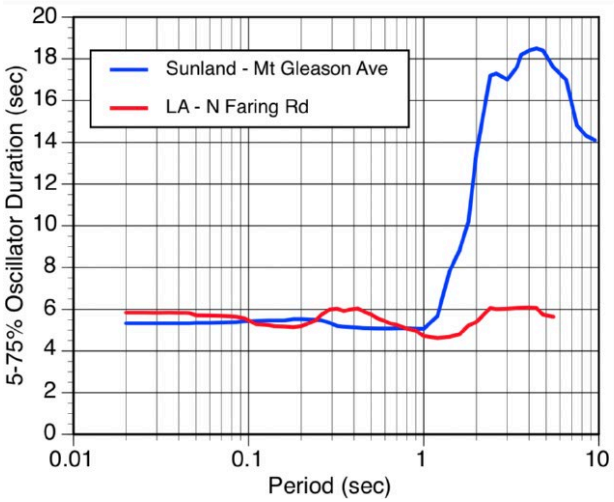

Figure 4. Example of period-dependent duration from two recordings of the 1994 Northridge earthquake with similar acceleration (short-period) durations but very different long-period durations.

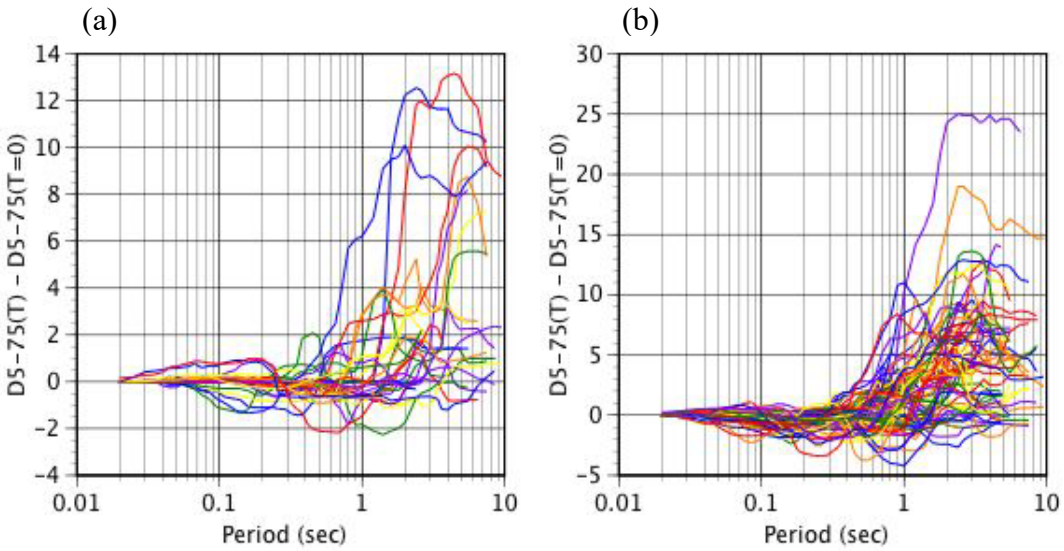

Figure 5. Period dependence of difference of the 5-75% oscillator duration and the 5-75% duration for acceleration for the 1994 Northridge earthquake. (a) Rupture distances of 0-20 km. (b) Rupture distances of 20-50 km.

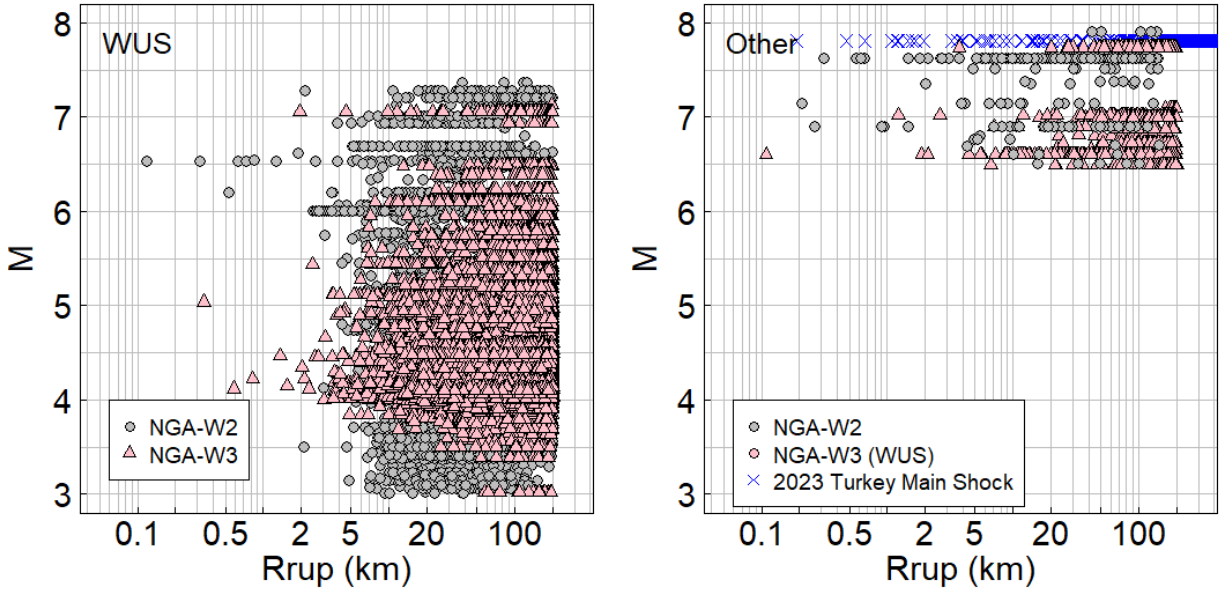

Figure 6. Selected data for developing the period-dependent duration model include (a) WUS events with M >= 3.0 and (b) global data with M >= 6.5 and R_{RUP} <= 200 m/s.

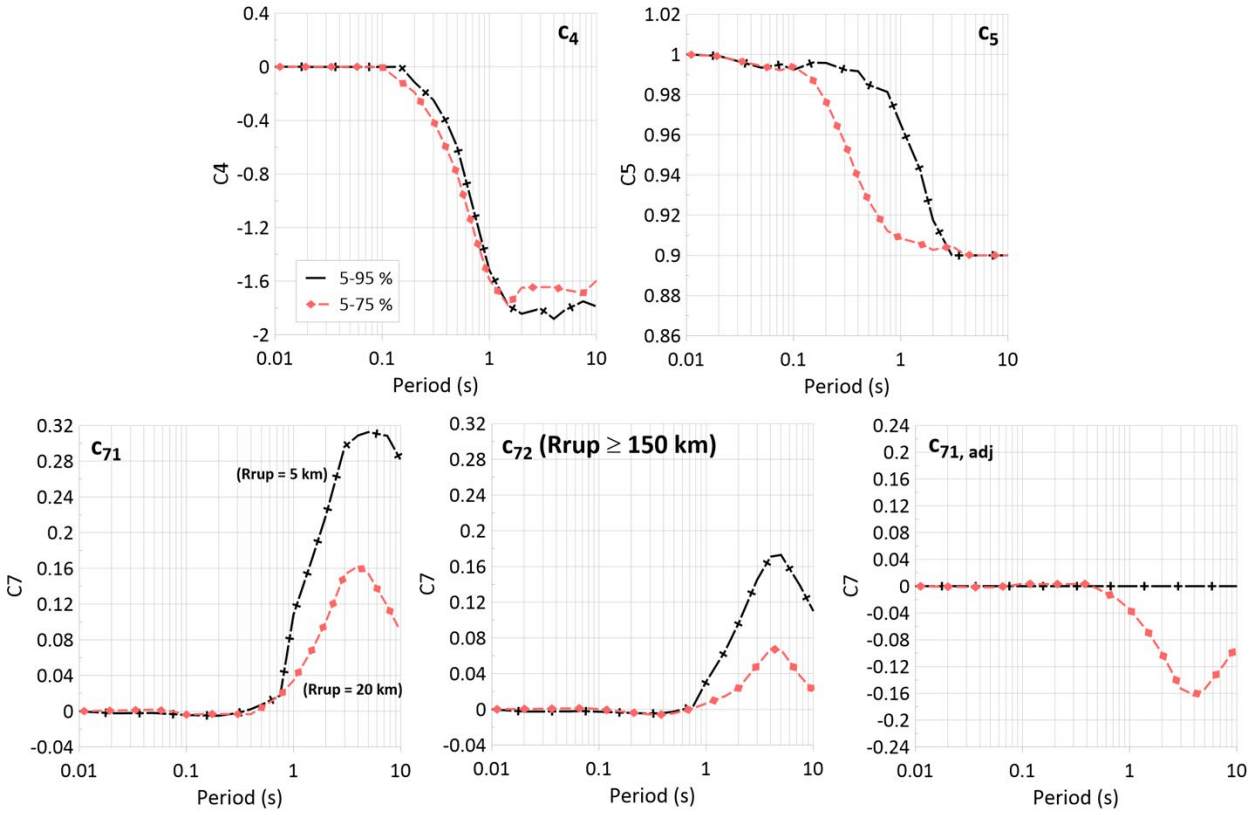

Figure 7. Coefficients for the period-dependent $D_{5\text{-}75}(T)$ and $D_{5\text{-}95}(T)$ models.

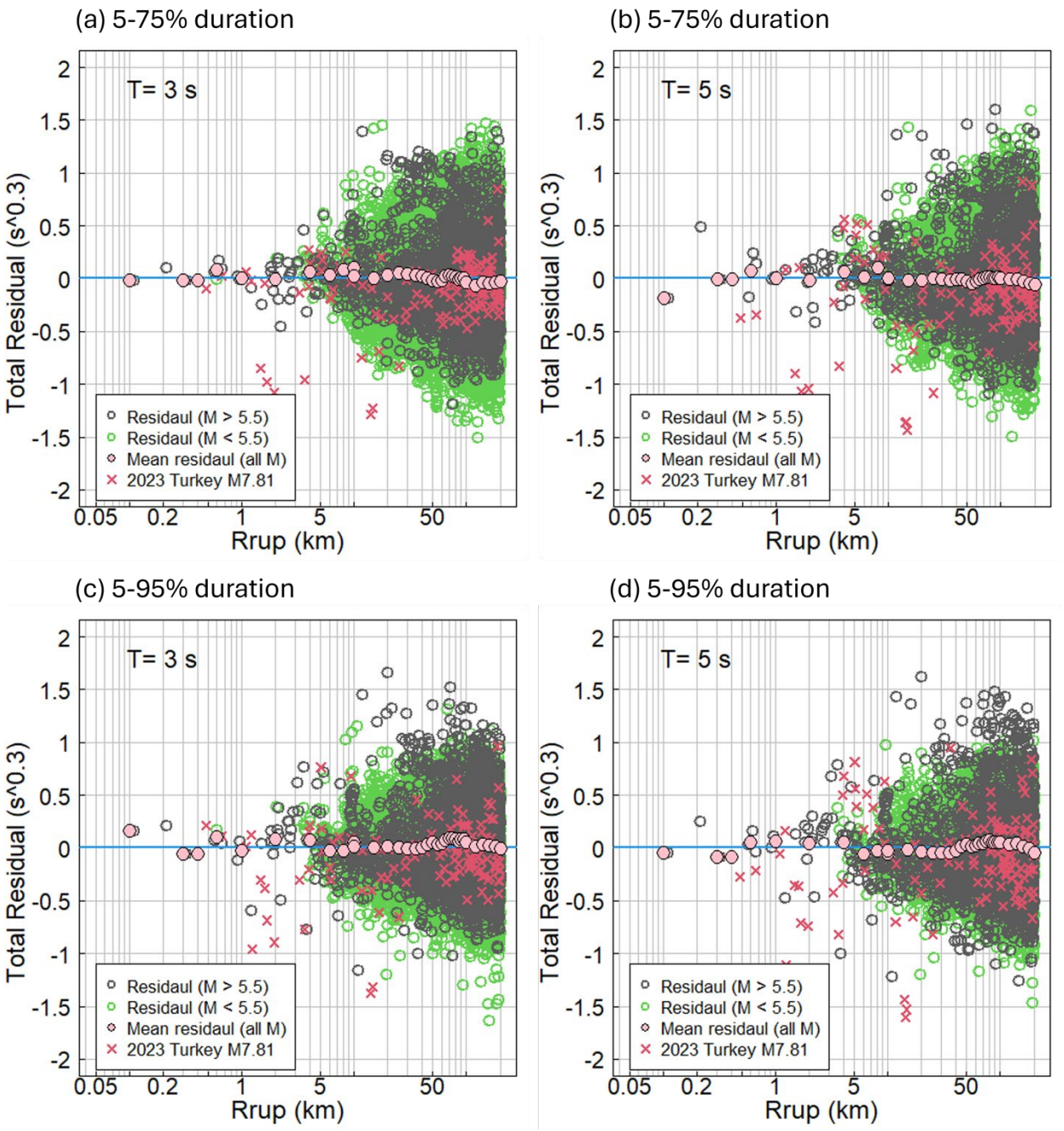

Figure 8. Residuals for the period-dependent $D_{5-75}^{0.3}(T)$ and $D_{5-95}^{0.3}(T)$ models for T=3 and T=5 sec. (a) $D_{5-75}^{0.3}(T=3)$, (b) $D_{5-75}^{0.3}(T=5)$, (c) $D_{5-95}^{0.3}(T=3)$, and (d) (c) $D_{5-95}^{0.3}(T=5)$

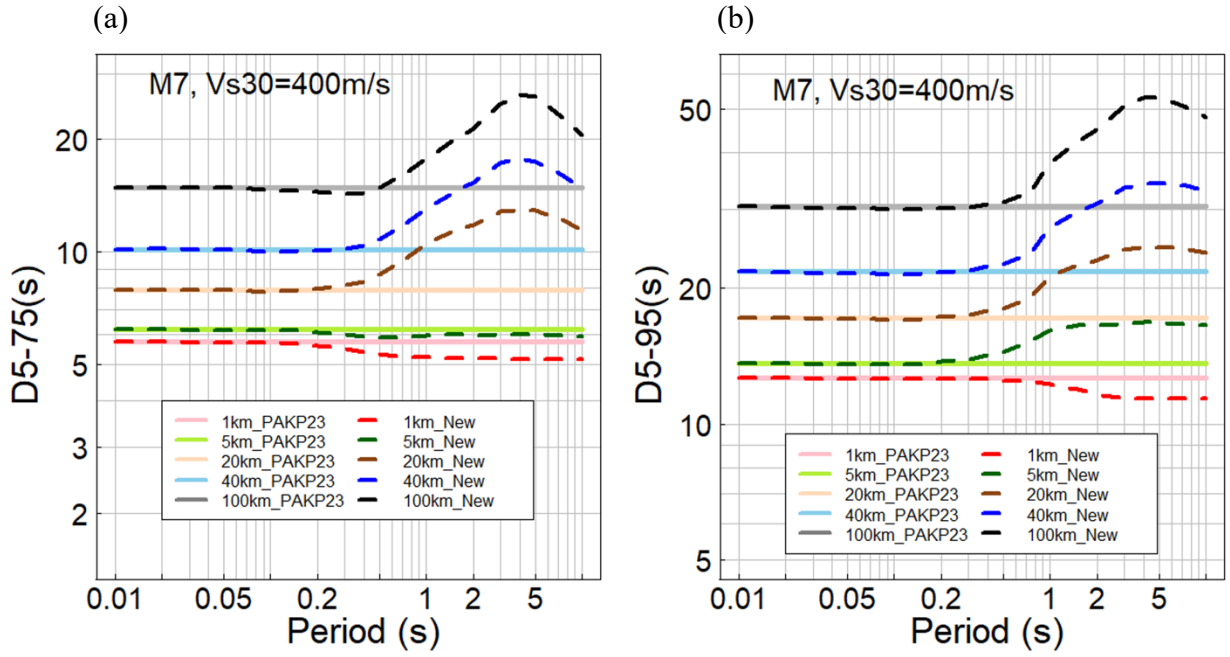

Figure 9. Comparison of the distance scaling for the acceleration duration from Pinilla-Ramos et al (2023) (solid lines) and the period-dependent duration (dashed lines) developed in this study. (a) $D_{5-75}(T)$ for M=7 and V_{S30}=400 m/s. (b) $D_{5-95}(T)$ for M=7 and V_{S30}=400 m/s.

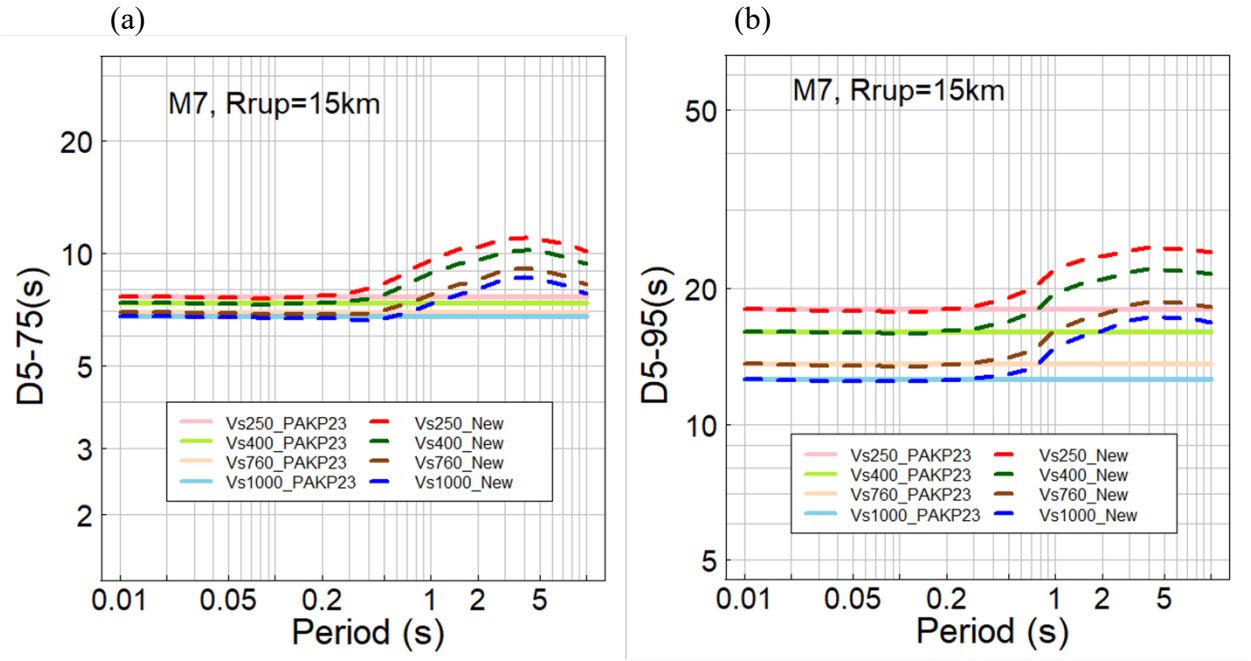

Figure 10. Comparison of the V_{S30} scaling for the acceleration duration from Pinilla-Ramos et al (2023) (solid lines) and the period-dependent duration (dashed lines) developed in this study. (a) $D_{5-75}(T)$ for M=7 and R_{RUP}=15 km. (b) $D_{5-95}(T)$ for M=7 and R_{RUP}=15 km.

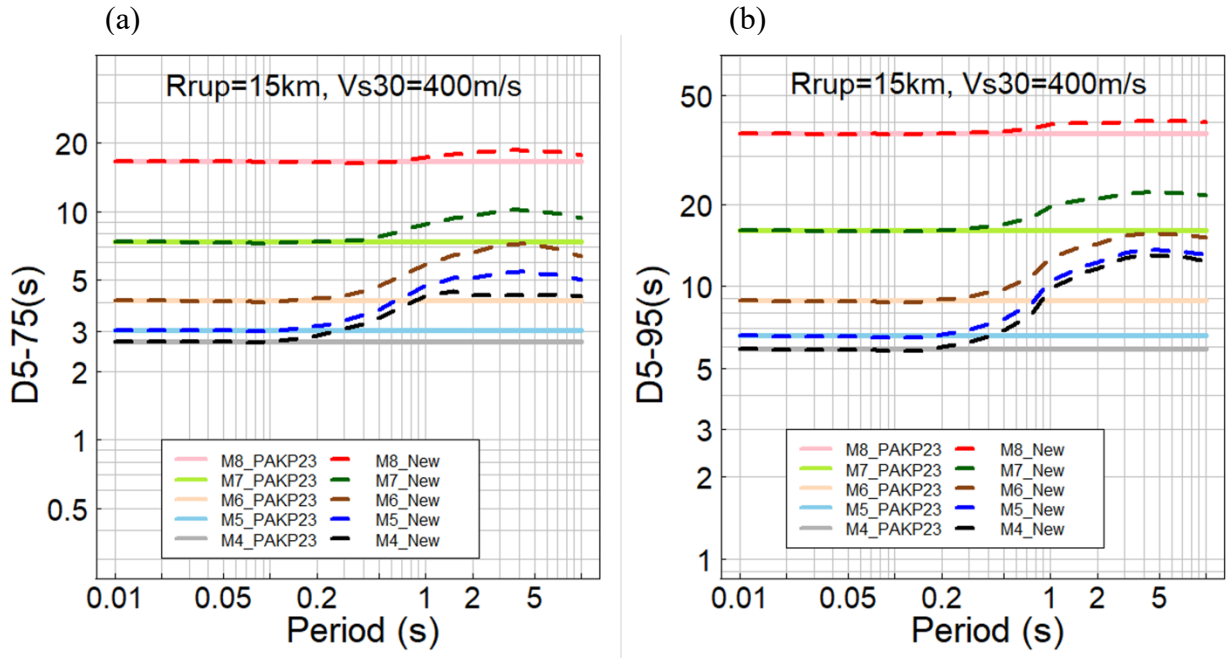

Figure 11. Comparison of the magnitude scaling for the acceleration duration from Pinilla-Ramos et al (2023) (solid lines) and the period-dependent duration (dashed lines) developed in this study. (a) $D_{5-75}(T)$ for R_{RUP}=15 km and V_{S30}=400 m/s. (b) $D_{5-95}(T)$ for R_{RUP}=15 km and V_{S30}=400 m/s.

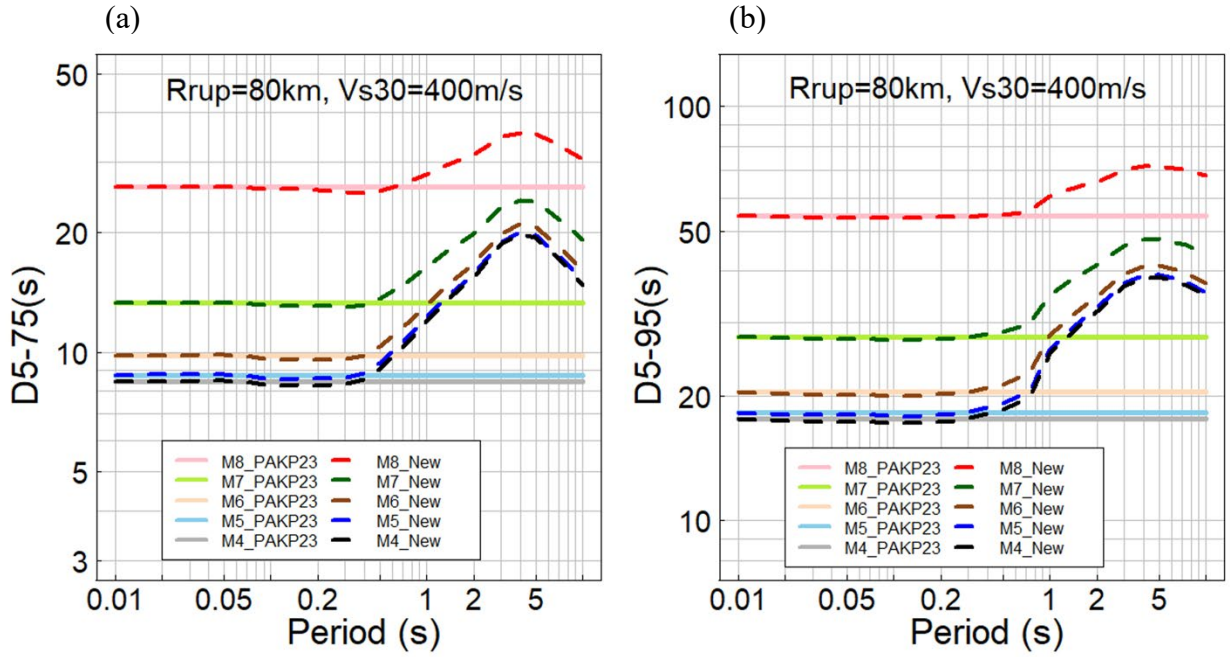

Figure 12. Comparison of the magnitude scaling for the acceleration duration from Pinilla-Ramos et al (2023) (solid lines) and the period-dependent duration (dashed lines) developed in this study. T(a) $D_{5-75}(T)$ for R_{RUP}=80 km and V_{S30}=400 m/s. (b) $D_{5-95}(T)$ for R_{RUP}=80 km and V_{S30}=400 m/s.

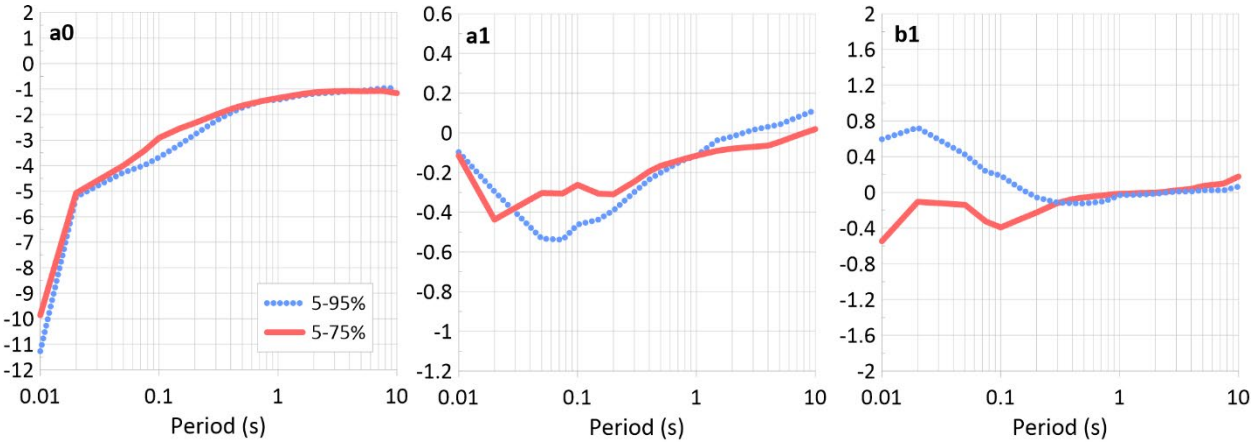

Figure 13. Coefficients for the standard deviation of the conditional period-dependent $D_{5\text{-}75}(T)$ and $D_{5\text{-}95}(T)$ models.

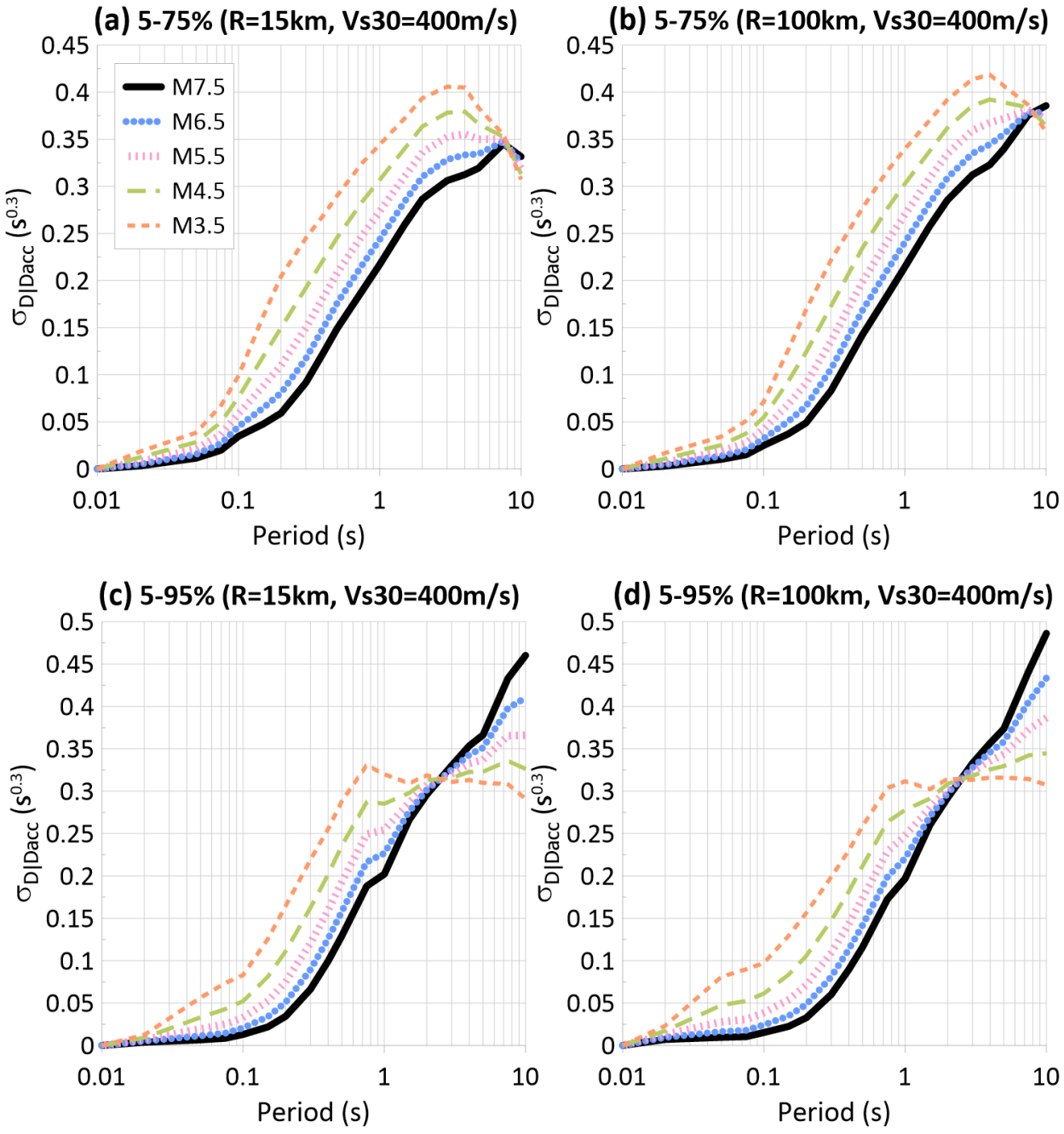

Figure 14. Period and magnitude dependence of the standard deviation of the conditional period-dependent $D_{5\text{-}75}(T)$ and $D_{5\text{-}95}(T)$ models (standard deviation given the acceleration duration. (a) and (c) are for $D_{5\text{-}75}$ and $D_{5\text{-}95}$ at R_{RUP}=15 km and the (b) and (d) are for $D_{5\text{-}75}$ and $D_{5\text{-}95}$ at R_{RUP}=100 km.

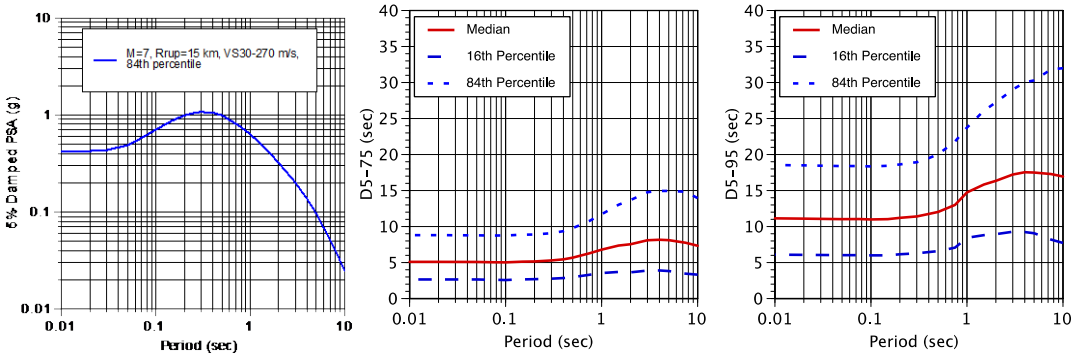

Figure 15. Example of the 84th percentile response spectrum for a scenario (M=7, Strike-slip, R_{RUP}=15 km, V_{S30}=270 m/s) and the corresponding duration spectra for the $D_{5\text{-}75}$ and $D_{5\text{-}95}$ duration. The duration spectra provide the target range of the period-dependent duration conditioned on the 84th percentile response spectrum and the M, R_{RUP}, and V_{S30} for this scenario.